Lemus, L., Harris, B., Bravo, A. and Rodríguez, J. (2025). Post-failure modelling of Las Palmas tailings dam using the Material Point Method. *Obras y Proyectos* **37**, 87-97
https://doi.org/10.21703/0718-2813.2025.37.3240

Post-failure modelling of Las Palmas tailings dam using the Material Point Method

Modelación del post-colapso del tranque de relaves Las Palmas usando el Método del Punto Material

Fecha de entrega: 10 de marzo 2025
Fecha de aceptación: 10 de abril 2025

Luis Lemus[1], Bryan Harris[1,2], Andrea Bravo[1] and Jaime Rodríguez[1]

[1] Universidad de La Serena, Departamento de Ingeniería en Obras Civiles, La Serena, Chile, llemus@userena.cl (Orcid: 0000-0003-3847-7819), bharris@alumnosuls.cl, abravoa@alumnosuls.cl, jrodrigu@userena.cl

[2] GHD Chile

In recent years, post-failure analysis has gained prominence in the geotechnical and mining industries for risk assessment and mitigation. Estimating runout from tailings dam failures is now a regulatory requirement for the design, operation, and closure of tailings storage facilities (TSFs). The key challenge lies in modelling large deformations while accounting for continuum soil mechanics. The Material Point Method (MPM), a continuum mechanics approach, shows promise due to its efficiency in modelling large deformations. It is particularly valuable for studying the entire instability process, including static stability, failure initiation, post-failure behaviour, and subsequent runout. This study applies MPM to a real case: the collapse of the Las Palmas tailings dam, triggered by the 2010 Maule earthquake in Chile (Mw 8.8). The dam is located approximately 30 km northwest of Talca, in Chile's Maule region. The computational model considers a two-dimensional plane-strain condition with fully saturated porous media and a coupled hydro-mechanical formulation. The results include velocity, deformation, displacement, and final deposition patterns. Notably, the computed runout distance aligns well with post-collapse field observations, validating the method's capability to replicate real cases. This research enhances our understanding of failure mechanisms and contributes to improved risk management in the mining industry.

Keywords: tailings dam failure, material point method, large deformation modelling

En los últimos años, el análisis post-colapso ha cobrado relevancia en la industria geotécnica y minera para la evaluación y mitigación de riesgos. La estimación del runout por fallas en presas de relaves se ha convertido en un requisito regulatorio para el diseño, operación y cierre de instalaciones de almacenamiento de relaves (TSF). El desafío clave radica en modelar grandes deformaciones considerando la mecánica de suelos del continuo. El Método del Punto Material (MPM), un enfoque de mecánica del continuo, muestra potencial debido a su eficiencia en el modelado de grandes deformaciones. Es particularmente valioso para estudiar todo el proceso de inestabilidad, incluyendo la estabilidad estática, el inicio de la falla, el comportamiento post-falla y el runout posterior. Este estudio aplica el MPM a un caso real: el colapso de la presa de relaves Las Palmas, desencadenado por el terremoto del Maule de 2010 en Chile (Mw 8.8). La presa está ubicada aproximadamente a 30 km al noroeste de Talca, en la Región del Maule, Chile. El modelo computacional considera una condición bidimensional de deformación plana con un medio poroso completamente saturado y una formulación hidromecánica acoplada. Los resultados incluyen patrones de velocidad, deformación, desplazamiento y deposición final. Cabe destacar que la distancia de runout calculada coincide con las observaciones in situ posteriores al colapso, lo que valida la capacidad del método para replicar casos reales. Esta investigación mejora nuestra comprensión de los mecanismos de falla y contribuye a una mejor gestión de riesgos en la industria minera.

Palabras clave: falla de presas de relaves, método de punto material, modelado de grandes deformaciones

Introduction

Tailings deposits are essential geotechnical structures in the mining industry. Despite high design standards, total or partial collapses still occur, primarily due to extreme natural events, operational management failures, and design deficiencies. In fact, tailings deposits have long been recognized as high-risk structures in terms of mechanical instability (Blight, 1997). A review of the main causes of tailings deposit failures worldwide indicates that they originate from large earthquakes, infiltration, overflow, and foundation soil instability (ICOLD, 2001; Davies, 2002; Rico *et al.*, 2008a; Azam and Li, 2010; Ishihara *et al.*, 2015; Villavicencio *et al.*, 2014). In Chile, the most significant failures are primarily caused by liquefaction (Dobry and Álvarez, 1967; Castro and Troncoso, 1989; GEER, 2010; Verdugo *et al.*, 2012; Kossoff *et al.*, 2014; Verdugo and González, 2015; Villavicencio *et al.*, 2014). This is attributed to various factors, such as Chile's highly seismic environment, upstream construction methodologies, and inadequate operational control. In general, liquefaction occurs when a large-magnitude, long-duration earthquake coincides with the presence of a water table or extensive saturated zones, and when the soil exhibits undrained behaviour under dynamic or static loads. In this context, high water content in a tailings deposit represents a critical and high-risk condition (Van Zyl, 2014).

Following the collapse of a tailings deposit, material flows downstream with great destructive power. Therefore, it is necessary to predict the flood zone, velocities, and flow path to develop mitigation measures and delineate safety zones. In this context, the concept of "dam-break analysis" has been adopted in various countries to predict the runout distance and inundation area of tailings after collapse. To quantify and manage this risk, it is essential to model both the rupture process and flow dynamics. This analysis is inherently complex because it requires integrating, within a single calculation, the transformation of solid material into a liquid or semi-liquid state, as occurs in liquefaction. Consequently, many computational models simplify the problem by treating tailings as a liquid material, which, in some cases, behaves as a viscous fluid.

To provide a practical solution for post-collapse analysis of these structures or similar landslides, several calculation methods have been developed. These include simplified numerical models (Jeyapalan *et al.*, 1981, 1983; Hungr, 1995) and empirical formulations based on historical failure data (Lucia *et al.*, 1981; Rico *et al.*, 2008b; Concha and Lall, 2018; Picciullo *et al.*, 2022). In recent decades, significant progress has been made in post-collapse analysis, leading to the development of computational models capable of predicting tailings flow kinematics. These models have been applied to various historical failure cases (Zabala and Alonso, 2011; Lumbroso *et al.*, 2021; Ghahramani *et al.*, 2022; Elkhamra *et al.*, 2023; Macedo *et al.*, 2024).

In Chile, catastrophic liquefaction-induced flow failures include the collapse of the El Cobre tailings dam in 1965, triggered by the La Ligua earthquake, and the collapse of the Las Palmas dam during the 2010 Maule earthquake. The latter case has been extensively studied (Bray and Frost, 2010; Gebarth, 2016; Moss *et al.*, 2019; Hernández, 2021; Quilodrán, 2021), demonstrating both numerically and experimentally that seismic-induced liquefaction was the mechanism responsible for the failure. In this context, this study contributes to understanding post-collapse behavior by considering flow failure. Through computational modeling, it proposes the use of the Material Point Method (MPM) to analyze the problem as one of large deformations.

The material point method

Numerous computational techniques have been developed to address large deformation issues in geotechnical engineering, with a particular focus on simulating failure initiation, its progression, and the subsequent runout. Among these methods, the Material Point Method (MPM) stands out as a promising approach, demonstrating successful applications in various hydro-mechanical coupled scenarios (Zabala and Alonso, 2011; Yerro *et al.*, 2013; Pinyol *et al.*, 2017; Lemus *et al.,* 2024). Originating from Sulsky *et al.* (1994, 1995), MPM is considered a hybrid method that integrates aspects of mesh-free techniques with traditional finite element method (FEM).

In MPM, the continuum is discretized into a collection of material points, each representing a subdomain and containing all relevant parameters, scalars, and vector fields. Additionally, a fixed background computational mesh is employed during calculations to solve the momentum equations across the entire problem domain over successive time steps. Utilizing standard interpolation functions from FEM, information is transferred and properties are updated between grid nodes and their corresponding material points at each incremental time step. This Eulerian-Lagrangian representation of the domain eliminates the need for mesh generation and regeneration, a common requirement in classical FEM approaches. For further details on the computational algorithm, readers are referred to Fern *et al.* (2019) and Soga *et al.* (2016) regarding geotechnical engineering applications. In this study, the governing

Lemus, L., Harris, B., Bravo, A. and Rodríguez, J. (2025). Post-failure modelling of Las Palmas tailings dam using the Material Point Method. *Obras y Proyectos* **37**, 87-97
https://doi.org/10.21703/0718-2813.2025.37.3240

equations used correspond to those formulated for fully saturated media, which are presented below.

A fully coupled saturated formulation in MPM is adopted here, and the 2-phase-1-point MPM approach to the dynamic behaviour of saturated porous media is considered within the framework of the generalized Biot formulation (Zienkiewicz and Shiomi, 1984). The v_S - v_L formulation (solid and liquid velocities) for saturated media in MPM was established by Jassim *et al.* (2013). The governing momentum balance equation for the liquid phase (per unit volume of liquid) is expressed as follows:

$$\rho_L a_L = \nabla p_L - \frac{n\mu_L}{k_L}(v_L - v_S) + \rho_L b \tag{1}$$

where a_L is the acceleration of the liquid phase, v_L and v_S are the total velocities of the liquid and solid phases, respectively, b is the body force vector, p_L is the liquid pressure, ρ_L is the density of the liquid phase, μ_L is the dynamic viscosity of the liquid, k_L is the intrinsic permeability of the liquid, and n is the porosity. This equation illustrates the so-called generalised Darcy's law.

The momentum balance of the mixture (per unit volume of the mixture) can be written as:

$$(1-n)\rho_S a_S + n\rho_L a_L = \nabla \bullet \sigma + \rho_m b \tag{2}$$

$$\rho_m = \rho_S(1-n) + \rho_L n \tag{3}$$

where a_S is the acceleration of the solid particles, σ is the Cauchy total stress tensor of the mixture, ρ_S is the density of the solid particles, ρ_n is the density of the mixture. The mass of the porous media must be separately conserved for each constituent in all calculations. In the case of the solid phase, the solid particles are considered incompressible ($\partial\rho_S/\partial t \approx 0$), therefore the conservation of mass of the solid phase becomes the following expression, which describes the material derivative of the porosity.

$$\frac{dn}{dt} - (1-n)\nabla \bullet v_S = 0 \tag{4}$$

The mass balance equation for the liquid phase can be written analogously to equation (4) as

$$\frac{dp_L}{dt} = \frac{K_f}{n}\left[\nabla \bullet v_L + (1-n)\nabla \bullet v_S\right] \tag{5}$$

where K_f is the liquid bulk modulus, equivalent to the reciprocal of the liquid compressibility ($K_f = -1/\beta_m$).

Post-failure modelling of Las Palmas tailing dam

The Las Palmas tailings dam is part of a former abandoned gold mining operation (Villavicencio *et al.*, 2014), located near the city of Talca in the Pencahue commune in the Maule Region, Chile (see Figure 1). After the earthquake that occurred in Chile on February 27, 2010, partial collapse of the Las Palmas mine tailings occurred, obstructing the local drainage network, and altering the local morphology due to the tailings flooding (Pizarro *et al.*, 2010; Verdugo *et al.*, 2010). Due to the seismic event, liquefaction occurred in its material, where this failure took two directions, one towards the East, with an approximate displacement of 165 m from the edge of the reservoir, and another towards the South, with an approximate displacement of 350 m from the edge of the reservoir (Figure 2). The liquefiable flow had an approximate thickness of 1.5 to 4.0 m in some places (Gebhart, 2016; Bray and Frost, 2010).The collapse was triggered by the interplate earthquake on February 27, 2010, with a magnitude of M_w 8.8 and a depth of 35 km off the coast of the Maule Region, ranking as the sixth largest earthquake recorded worldwide since 1900.

Figure 1: Location of the Las Palmas Tailings Dam. Source: Modified from Google Earth, 2023

A liquefaction failure was observed at the base level of the retaining dam, apparently due to saturation of the few lower meters (0.5 to 1 m) caused by undetected groundwater. This saturation zone apparently was not detected at the time of the closure of the deposit (Villavicencio *et al.*, 2014).

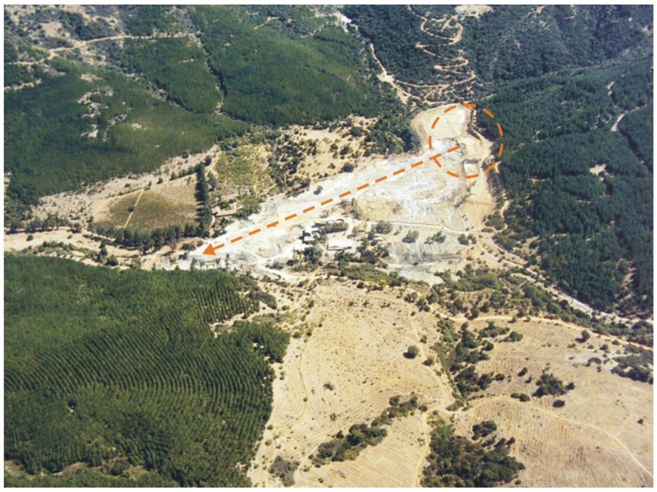

Figure 2: Las Palmas tailings dam after the collapse generated by the 27 February 2010 earthquake (Villavicencio *et al.*, 2014)

Geometric and construction stages configuration

The tailings dam was built on a terrain with a slope descending towards the South and East. Above, it had a maximum upper slope of 4:1 (horizontal and vertical) and a maximum lower slope of 15:1, horizontal and vertical (Gebhart, 2016). In Figure 3 is showed the construction sequence of the dam, which consisted of 4 individual stages developed over a period of 17 years, between 1981 and 1998 (Moss *et al.*, 2019; Gebhart, 2016). The sequence began with the construction of stage one, which consisted of a retaining wall and placement of hydraulic fill tailings (finely crushed solid). Following this, as shown in Figure 3, stage two was positioned upstream at the same height as the initial wall. Subsequently, on these two completed stages, and using the downstream method, stage three was constructed. Finally, in stage four, walls and tailings were positioned on the material contained in stage three. For the case of retaining walls or embankments, the sandy and granular fraction of the tailing's material was used to generate greater resistance capacity.

To generate the surface of soil foundation, a two-dimensional model is created prior to the failure, along with Google Earth satellite images supplemented with a raster model of the area, to obtain the corresponding contour lines of the terrain using QGIS software as showed in the Figures 4 and 5.

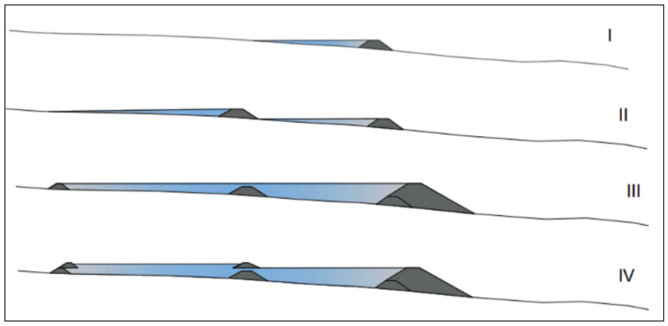

Figure 3: Construction stages of Las Palmas Tailing dam (Pizarro *et al.*, 2010)

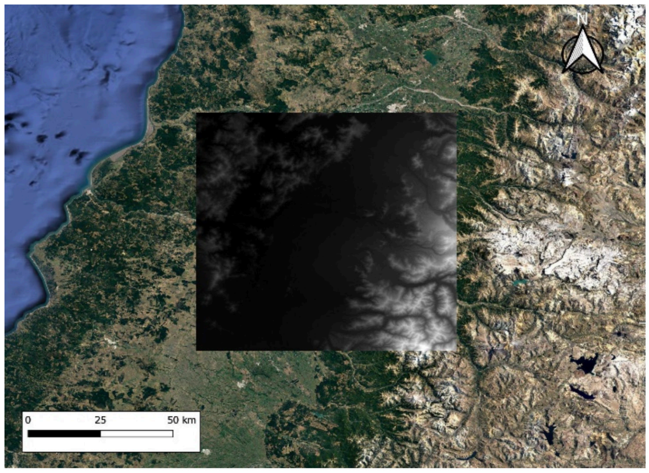

Figure 4: Raster and contour lines of the Las Palmas tailings sector.

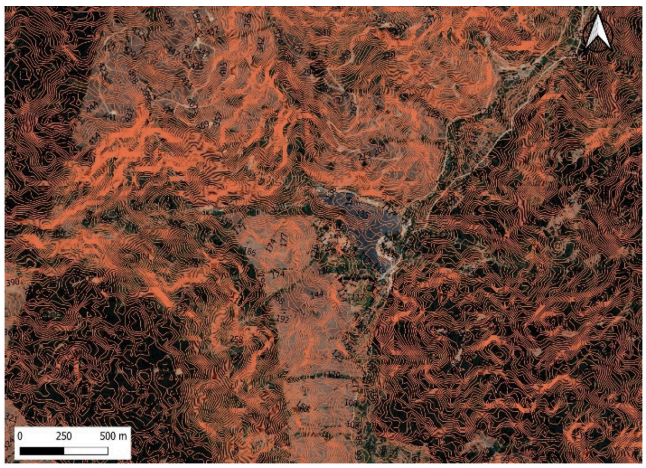

Figure 5: Contour lines generated in QGIS.

With the above information, the slopes where the collapsed material moved were traced, complementing with the geometry of the tailings dam prior to the failure obtained from Hernández (2021). Subsequently, the geometric digital model shown in Figure 7 was developed using

Lemus, L., Harris, B., Bravo, A. and Rodríguez, J. (2025). Post-failure modelling of Las Palmas tailings dam using the Material Point Method. *Obras y Proyectos* **37**, 87-97
https://doi.org/10.21703/0718-2813.2025.37.3240

AutoCAD Civil 3D software corresponding to the section indicated in Figure 6.

Figure 6. Top view and profile line prior to the failure (Gebhart, 2016)

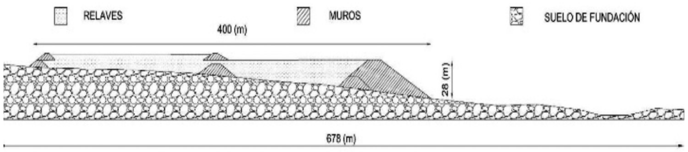

Figure 7: Cross-sectional profile of the two-dimensional geometric model of the Las Palmas tailings dam prior to the failure.

Geotechnical characterization and adopted parameters

According to the drilling records, triaxial tests, geotechnical characterization, and the post-collapse reconnaissance work of the deposit (Bray and Frost, 2010; Gebhart, 2016), it was determined that the computational model considered three types of materials: tailings, walls, and foundation soil. The tailings from the dam are composed of a sandy silt material with a low percentage of silty sand susceptible to liquefaction. The constitutive model used for the tailings corresponds to the classical Mohr Coulomb model for both liquefied and non-liquefied material.

Non-Liquefied Tailings: For modelling the non-liquefied tailings material, a drained condition was considered (cohesion of 0 kPa), where, due to the frictional resistance of the silts, "peak" and residual parameters of this material were obtained. The residual parameters were chosen to determine the internal friction angle corresponding to 21°, as it best represented the mobilized soil resistance within the flow failure. The Young's modulus was calculated considering the number of blows from the drillings obtained from the data provided by Gebhart (2016), resulting in different modulus values from which an average value of 1341 kPa was calculated to represent the material. As for Poisson's ratio, a value of 0.325 was adopted from specialized literature considering various soil classifications.

Liquefied Tailings: The liquefied tailings material has a residual post-liquefaction strength of 8.28 kPa obtained from the conclusions of Gebhart (2016). It has a friction angle of 0° due to the deficiency in its load-bearing capacity if the material liquefied entirely due to the seismic event. For the Young's modulus, Poisson's ratio, and other parameters, the same values as the non-liquefied tailings were retained.

Sand walls: The material used to construct the walls or containment dikes is classified as silty sand (SM) with a low percentage of silt. In the models created, it was configured using the classical Mohr Coulomb constitutive model.

Non-Liquefied walls: Regarding the parameters of this material, a friction angle of 26° and a cohesion of 38.3 kPa were assigned, obtained from triaxial tests under consolidated undrained conditions. The Young's modulus of 5724 kPa, similar to the tailings, was obtained from the number of blows/foot of the SPT test conducted in situ. Poisson's ratio of 0.3 was defined based on existing tables in specialized literature associated with various soil classifications.

Liquefied sand walls: the parameters of Young's modulus (E) and Poisson's ratio (ν) remain unchanged. As for cohesion, a low value is assigned because it is assumed that the collapsed material had no resistance due to the seismic event, with a value of 3 kPa.

Soil foundation: for the analyzed case study it was considered as a competent material with high strength that had minimal relevance in the collapse of the deposit. Regardless of this assessment, the material was configured with a linear elastic model with a very high modulus of elasticity to represent it as an impenetrable material. Based on the review of background information, it was confirmed that no failure occurred in the foundation soil, validating the assumption that this material has high strength.

According to this, a resume of adopted parameters is shown in Table 2.

Table 2: Summary of parameters adopted for the model in MPM.

Parameter	Non-liquefied sand walls	Liquefied sand walls	Non-liquefied tailings	Liquefied tailings	Soil foundation
n	0.65	0.65	0.65	0.65	0.25
ρ_s , kg/m^3	2730	2730	2730	2730	2700
ρ_l , kg/m^3	1000	1000	1000	1000	1000
k_L, m^2	1.0 x 10^{-8}	1.0 x 10^{-8}	1.0 x 10^{-8}	1.0 x 10^{-8}	1.0 x 10^{-5}
K_f, kPa	2.2 x 10^{-4}	2.2 x 10^{-4}	2.2 x 10^{-4}	2.2 x 10^{-4}	2.2 x 10^{-4}
μ, kPa·s	1.0 x 10^{6}	1.0 x 10^{6}	1.0 x 10^{6}	1.0 x 10^{6}	1.0 x 10^{6}
ν	0.3	0.3	0.325	0.325	0.2
E, kPa	5724	5724	1341	1341	200000
c, kPa	38.3	5	0	8.28	-
φ , º	26	3	21	0	-

ρ_s: solid density; ρ_l: liquid density; n: porosity; k_L: Intrinsic permeability; K_f: bulk modulus of water; μ: dynamic viscosity; E: Young modulus; ν: Poisson's ratio; c: cohesion; φ: friction angle

Model configurations and computational meshing

Two calculation phases are considered: a static phase is performed by the application of gravity loading and a dynamic phase corresponds to the collapse. In the Anura3D code, calculation data were established to evaluate the number of time steps (iterations) to be calculated. Each calculation step represents a fraction of time, which in this case was determined to be equivalent to 0.1 s per step. Considering a total of 600 time-steps, therefore the real simulation time is 60 s.

The two-dimensional model mesh encompasses the entire computational domain, even where there is initially no material (blue mesh), as depicted in Figure 8. The objective is to fully cover the spatial domain where it is assumed that material will exist when the soil mass moves. In all models created, the mesh consists of triangular linear elements, as shown in Figure 8. For the analyzed deposit, the dimension of the foundation soil elements was set to 5.0 m as it is not relevant in the modelling (unnecessary and time-consuming calculations), while for the tailings, walls, and areas where material could mobilize, it was set to 1.5 m. Additionally, an unstructured mesh of 1.0 m was applied to the interface line between the collapsed tailings and the foundation soil, achieving mesh refinements in the areas of interest (where the material will mobilize) to attain a refined calculation network and avoid interference from overly coarse mesh in the flow of collapsed material. This model consists of 13674 nodes and 26690 triangular elements, each of which is composed of three material points equivalent to a total of 80070 particles.

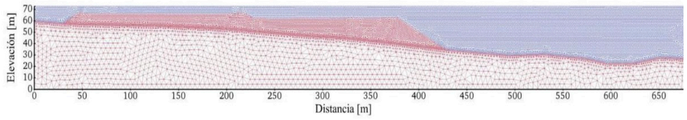

Figure 8: Computational mesh of the model

The MPM is implemented in Anura3D opensource code (Anura Research Community 2022) in Fortran language. To the simulations in a virtual machine with high calculation performance. The characteristic of the CPU used is detailed in Table 3.

Table 3: CPU characteristics of virtual machine used

CPU details	
Operating System	Windows 10 Pro, v. 22H2, 64 bits, processor x64
Processor	Intel® Xeon® Gold 52218 CPU @ 2.30GHz
N° cores	12 Cores de CPU
Storage	500 Gb
Memory (RAM)	64 Gb

Results

A static calculation phase is presented, corresponding to the initialization of stress state by quasi-static gravitational loads, defined in two calculation steps. The result at the end of this phase is shown in Figure 9.

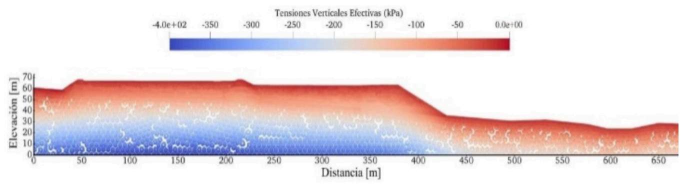

Figure 9: Vertical geostatic stress due to initial conditions setting.

The dynamic stage of the model corresponds to the displacement of the materials composing the tailings dam, where one of the objectives of this study is the analysis of the post-collapse scenario. A total of 600 calculation steps, corresponding to 60 s after the static phase, were considered, as this is an appropriate time range for complete collapse to occur and for the runout distance to be obtained.

Lemus, L., Harris, B., Bravo, A. and Rodríguez, J. (2025). Post-failure modelling of Las Palmas tailings dam using the Material Point Method. *Obras y Proyectos* **37**, 87-97
https://doi.org/10.21703/0718-2813.2025.37.3240

Here the liquefied parameters were used for both the tailings and the downstream walls of the dam. Given the magnitude of a seismic event, it is assumed that the tailings, being very fine and barely compacted materials, liquefy entirely. In the case of the walls, liquefaction was considered as there are records confirming their collapse. Regarding the central walls and those located upstream, they remained in non-liquefied conditions as observed in situ, maintaining their initial position, thus preserving the quasi-static parameters. Figure 10 illustrates the material conditions at the start of the dynamic phase of the model.

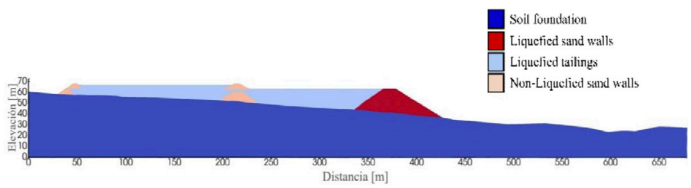

Figure 10: Material configuration of the model.

During the dynamic phase, of the initial 60 s of time considered, it only took 49 s for the material to come to a stop, allowing the run-out distance to be visualized. Within this time interval, the material traveled 160 m from the toe of the downstream wall slope (see Figures 11 and 12).

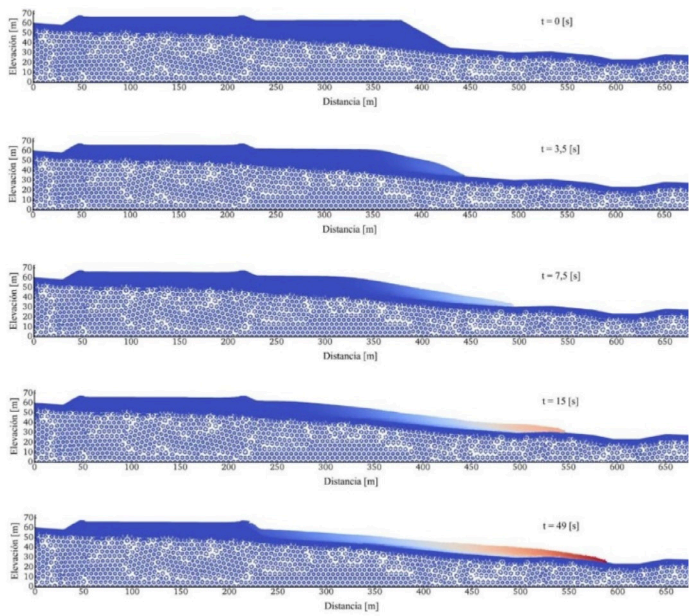

Figure 11: Evolution of position of tailing dam flow failure.

According to the information gathered, the collapsed material reached an approximate distance of 165 m. When comparing this result with the computational model, there

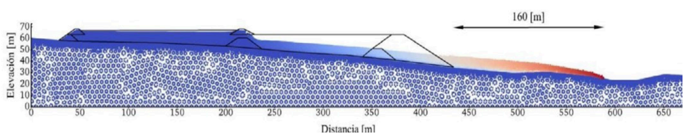

Figure 12: Final deposition of collapsed tailings and initial geometric setup.

is agreement in terms of runout distance reached. The difference could be attributed to the fact that, since the focus of dam modelling was on post-collapse behaviour, seismic analysis was not considered. It was assumed that both the tailings and the downstream walls liquefied. Additionally, due to the lack of exact knowledge of some material parameters, common values for a certain soil classification had to be used, and assumptions were made for values for which there were no data.

Additionally, it is observed that during the collapse, the downstream walls (coarse material), as depicted in Figure 13, began to open a path along the slope of land surface. However, during the movement, particles were left behind along the path, causing the tailings (fine material) to spread over the liquefied material of the walls but not to surpass it. Additionally, it is evident that the tailings upstream did not flow due to the non-liquefied parameters of the central walls. Nevertheless, it is observed that the wall in stage IV (central), despite its properties, exhibited deformations in its structure.

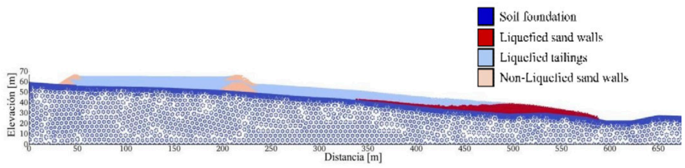

Figure 13: Final disposal of constituent materials after the collapse.

The volumetric deformations during the geostatic phase are shown in Figure 14(a), where small deformation values can be observed, as the materials in this condition still possess a level of non-liquefied material resistance. However, already in the early moments of the dynamic phase, shear bands are evidenced at the interfaces and into the principal sand wall (see Figure 14(b)). Following this, the deformation began to progress backwards, where the shear bands gradually increased due to the liquefied tailings until it completely lost its resistance, causing it to descend as a whole or in block form. At the same time, it is observed how the bands ascended along the slope of the lower central wall until reaching the point of generating deformations and subsequent rupture of the upper wall, as shown in Figure 14(c), that agree with the real case (see Figure 15).

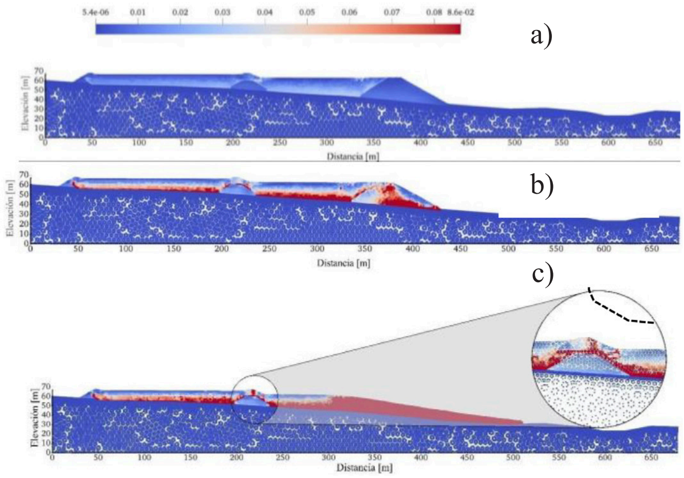

Figure 14: Volumetric deformation and shear bands at the failure initiation.

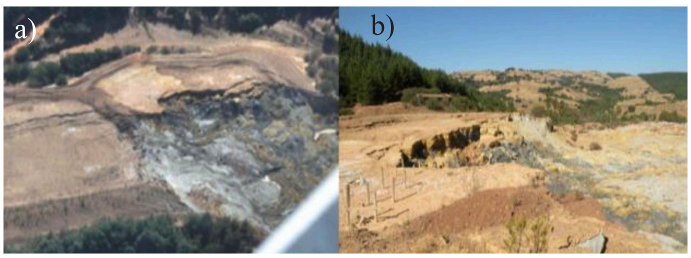

Figure 15: State of the central walls post-collapse (Gebhart, 2016; Bray and Frost, 2010. a) Aerial view of the walls and the material and b) edge of mobilized flow failure.

The description of the tailings flow kinematics is conducted through the tracking of control points located in different areas of the deposit. These control points are indicated in Figure 16, where it can be observed that there are differences in the velocities reached, both in terms of magnitude and timing of occurrence. Maximum velocities can be observed at different time instants. Regarding the advance front of the tailings, an average of maximum values is 14 m/s (~ 50 km/h) reached at about 7 s, highlighting the destructive power of tailing flow that was developed (see Figure 16).

Finally, the displacements of three control points are analyzed, which are indicated in Figure 17, along with their respective evolution over time. The maximum displacement reached is around 180 m in the "Point 3" located at the slope of the dam (see Figures 17 and 18). Regarding the displacement of "Point 1" (tailings material), it is inferred

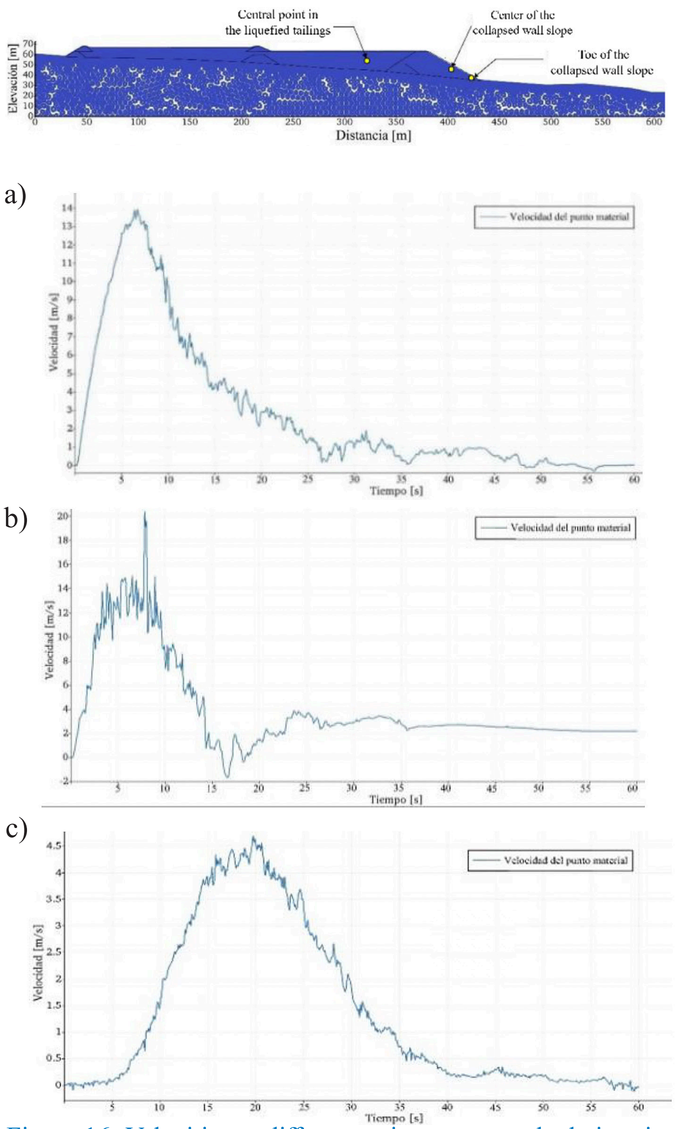

Figure 16: Velocities at different points versus calculation time. a) Central point in liquefied tailings, b) center of the collapsed sand wall, and c) toe of the collapsed sand wall.

that at approximately 7 s, the material begins to slide, where it is observed that at 33 s, a maximum displacement of 70.2 m is generated. After this, the particles begin to stabilize.

As for "Point 2" and "Point 3," corresponding to the collapsed wall, a significant difference can be appreciated between their values due to their positions. "Point 3" shows a pronounced curve because in the first 10 s, the material moved approximately 100 m, reaching the maximum collapse displacement (179.8 m) at 49 s. The reason for this is that being on the downstream slope of the collapsed wall leads to greater movement from the beginning of the failure without resistance from a material holding it back. On the other hand, "Point 2" only traveled 2.88 m, starting its movement at approximately 13 s and stopping at 35 s. This is because it is located at the back of the base of the wall, causing the tailings material to pass over this point, reducing its displacement.

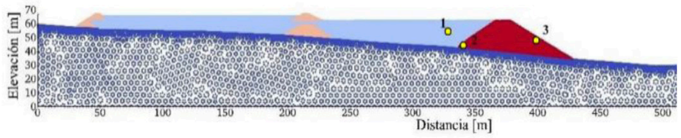

Figure 17: Points selected for displacements analysis.

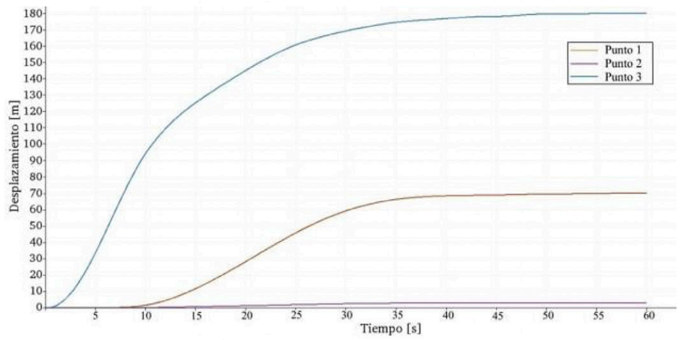

Figure 18: Displacements over time for three points.

Conclusions

This study enhances the applicability of the Material Point Method (MPM) for understanding the behaviour of tailings deposits after failure, leveraging its unique capabilities for modelling large soil deformations. The results obtained for travel distance are validated against field data collected after the deposit collapse. In this regard, an estimated runout distance of approximately 160 m from the toe of the sand wall slope aligns well with observed data. However, at another location, into the tailing dam, the maximum calculated displacement reaches approximately 180 m.

Regarding the failure evolution in terms of deformations and shear band formation, the collapse morphology—influenced by the assumption of liquefied material parameters during the dynamic phase— was successfully replicated. Additionally, the model's velocity estimates are particularly noteworthy, as they contribute to validating the destructive potential of the tailings flow. Nevertheless, there remains room for improvement in describing the failure process, which could be achieved by incorporating advanced constitutive models that explicitly account for liquefaction under seismic loading.

Future research should focus on further improving the proposed model. This could involve integrating a more advanced constitutive model to enhance the accuracy of tailings behaviour predictions and seismic liquefaction-induced failures. Additionally, with appropriate computational implementation, a finer mesh could be employed to minimize interference from an overly coarse discretization in the flow of collapsed material. Increasing the number of material points per triangular element could also help mitigate numerical instabilities. Finally, incorporating seismic loading conditions and dynamic parameters, as well as developing a three-dimensional computational model, would enhance the model's reliability and improve its predictive capabilities for future failures.

Acknowledgements

The authors would like to thank the Department of Civil Engineering at the University of La Serena for their support in this work. Luis Lemus acknowledges the National Agency for Research and Development (ANID) of the Government of Chile for the doctoral scholarship abroad (CONICYT-PCHA/Doctorado Internacional/2017-72180231) and to the financial support of FIULS 2030 through the project "FIULS 2030", code 18ENI2-104235, from the program "New Engineering for 2030 in Regions - Implementation Stage.

References

Anura3D (2022). MPM Research Community. https://github.com/Anura3D/Anura3D_OpenSource

Azam, S. and Li, Q. (2010). Tailings dam failures: a review of the last one hundred years. Geotechnical News/Waste Geotechnics, 50-53

Blight, G. (1997). Destructive mudflows as a consequence of tailings dyke failures. *Proceedings of the ICE – Geotechnical Engineering* **125**(1), 9–18

Bray, J.D. and Frost, J.D. (eds.) (2010). Geo-engineering Reconnaissance of the 2010 Maule, Chile Earthquake. Geo-engineering Extreme Events Reconnaissance GEER Association, Report No. GEER-022, USA

Castro, G. and Troncoso, J. (1989). Effects of 1985 Chilean earthquake on three tailing dams. *Fifth Chilean Conference on Seismology and Earthquake Engineering*, Santiago, Chile

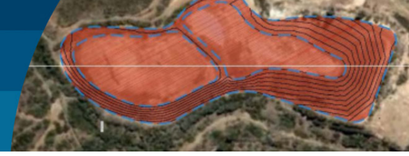

Concha, P. and Lall, U. (2018). Tailings dams failures: Updated statistical model for discharge volume and runout. *Environments* **5**(2), 28

Davies, M.P. (2002). Tailings impoundment failures: are geotechnical engineers listening?. Geotechnical News/Waste Geotechnics, 31–36

Dobry, R. and Alvarez, L. (1967). Seismic failures of Chilean tailings dams. *Journal of the Soil Mechanics and Foundations Division* **93**(6), 237–260

Elkhamra, Y., Chen, H. and Stark, T. (2023). Inverse analysis of Cadia tailings dam failure. *Geo-Congress 2023*, E. Rathje, B.M. Montoya and M.H. Wayne (eds.), ASCE and GI, Los Angeles, CA, USA, 10-19

Fern, J., Rohe, A., Soga, K. and Alonso, E. (eds.). (2019). *The Material Point Method for Geotechnical Engineering: A Practical Guide*. CRC Press, Taylor & Francis Group, Boca Raton, USA

GEER (2010). Dams, levees, and mine tailings dams. Turning disaster into knowledge: geo-engineering reconnaissance of the 2010 Maule, Chile Earthquake. Geo-Engineering Extreme Events Reconnaissance Association GEER. J. Bray and D. Frost (eds.), 204–226

Gebhart, T.R. (2016). *Post-liquefaction residual strength assessment of the Las Palmas, Chile tailings failure*. MSc thesis, California Polytechnic State University, San Luis Obispo, USA

Ghahramani, N., Chen, H.J., Clohan, D., Liu, S., Llano-Serna, M., Rana, N.M., McDougall, S., Evans, S.G. and Take, W.A. (2022). A benchmarking study of four numerical runout models for the simulation of tailings flows. *Science of the Total Environment* **827**, 154245

Hernández, A.B. (2021). *Colapso del tranque de relaves Las Palmas durante el sismo del Maule 2010*. Tesis de magíster, P. Universidad Católica de Chile, Macul, Chile

Hungr, O. (1995). A model for the runout analysis of rapid flow slides, debris flows, and avalanches. *Canadian Geotechnical Journal* **32**(4), 610–623

ICOLD (2001). Tailings dams - risk of dangerous occurrences, lessons learnt from practical experiences. Bulletin 121. United Nations Environmental Programme (UNEP), Division of Technology, Industry and Economics (DTIE) and International Commission on Large Dams (ICOLD), Paris, France

Ishihara, K., Ueno, K., Yamada, S., Yasuda, S. and Yoneoka, T. (2015). Breach of a tailings dam in the 2011 earthquake in Japan. *Soil Dynamics and Earthquake Engineering* **68**, 3–22

Jassim, I., Stolle, D. and Vermeer, P. (2013). Two-phase dynamic analysis by material point method. *International Journal for Numerical and Analytical Methods in Geomechanics* **37**(15), 2502–2522

Jeyapalan, J.K., Duncan, J.M., Seed, H.B. (1981). Summary of research on analyses of flow failures of mine tailings impoundment. Information Circular 8857, Technology Transfer Workshop on Mine Waste Disposal Techniques, US Bureau of Mines, Denver, CO, USA, 54–61

Jeyapalan, J.K., Duncan, J.M. and Seed, H.B. (1983). Analyses of flow failures of mine tailings dams. *Journal of Geotechnical Engineering* **109**(2), 150–171

Kossoff, D., Dubbin, W.E., Alfredsson, M., Edwards, S.J., Macklin, M.G., Hudson-Edwards, K.A. (2014). Mine tailings dams: characteristics, failure, environmental impacts, and remediation. *Applied Geochemistry* **51**, 229–245

Lemus, L., Rodríguez, J., Cáceres, V. y Mery, D. (2024). Modelación computacional de deslizamientos de tierra masivos inducidos por sismos usando el Método del Punto Material. *Obras y Proyectos* **35**, 31-39

Lucia, P.C., Duncan, J.M. and Seed, H.B. (1981). Summary of research on case histories of flow failures of mine tailings impoundments. Technology Transfer Workshop on Mine Waste Disposal Techniques, US Bureau of Mines, Denver, CO, USA, 46-53

Lumbroso, D., Davison, M., Body, R. and Petkovšek, G. (2021). Modelling the Brumadinho tailings dam failure, the subsequent loss of life and how it could have been reduced. *Natural Hazards and Earth System Science* **21**, 21–37

Macedo, J., Yerro, A., Cornejo, R. and Pierce, I. (2024). Cadia TSF failure assessment considering triggering and posttriggering mechanisms. *Journal of Geotechnical and Geoenvironmental Engineering* **150**(4), 04024011

Moss, R.E.S., Gebhart T.R., Frost J.D. and Ledezma C. (2019). Flow-failure case history of the Las Palmas, Chile, tailings dam. Pacific Earthquake Engineering Research Center PEER report 2019/01. UC Berkeley, USA

Piciullo, L., Storrøsten, E.B., Liu, Z., Nadim, F. and Lacasse, S. (2022). A new look at the statistics of tailings dam failures. *Engineering Geology* **303**, 106657

Pinyol, N.M., Alvarado, M., Alonso, E.E. and Zabala, F. (2017). Thermal effects in landslide mobility. *Géotechnique* **68**(6), 528-545

Pizarro, G., Pastén, P., Bonilla, C., Tarud, F. y Acevedo, S. (2010). Evaluación preliminar de contingencia en tranque de relaves Las Palmas, Sector Pencahue, Región del Maule. DICTUC, Macul, Chile

Quilodrán, C.A. (2021). *Distancia peligrosa tranque de relaves Las Palmas*. Tesis de magíster, P. Universidad Católica de Chile, Macul, Chile

Rico, M., Benito G., Salgueiro A.R., Díez-Herrero A. and Pereira H.G. (2008a). Reported tailings dam failures a review of the European incidents in the worldwide context. *Journal of Hazardous Materials* **152**(2) 846–852

Rico, M., Benito G. and Díaz-Herrero A. (2008b). Floods from tailings dam failures. *Journal of Hazardous Materials* **154**(1-3), 79–87

Soga, K., Alonso, E., Yerro, A., Kumar, K. and Bandara, S. (2016). Trends in large-deformation analysis of landslide mass movements with particular emphasis on the material point method. *Géotechnique* 66(3), 248–273

Sulsky, D., Chen, Z. and Schreyer, H.L. (1994). A particle method for hystory-dependent materials. *Computer Methods in Applied Mechanics and Engineering* **118**(1-2), 179–196

Sulsky, D., Zhou, S.J. and Schreyer, H.L. (1995). Application of a particle-in-cell method to solid mechanics. *Computer Physics Communications* **87**(1-2), 236–252

Van Zyl, D. (2014). Plenary Presentation: Holistic approach to mine waste management. *2nd International Seminar on Tailings Management*, Gecamin: Tailings 2014, Antofagasta, Chile

Verdugo, R. and González, J. (2015). Liquefaction-induced ground damages during the 2010 Chile earthquake. *Soil Dynamics and Earthquake Engineering* **79**, 280–295

Verdugo, R., Sitar, N., Frost, J.D., Bray, J.D., Candia, G., Eldridge, T., Hashash, Y., Olson, S.M. and Urzua, A. (2012). Seismic performance of earth structures during the February 2010 Maule, Chile, earthquake: dams, levees, tailings dams, and retaining walls. *Earthquake Spectra* **28**(1), 75-96

Verdugo, R., Villalobos, F., Yasuda, S., Konagai, K., Sugano, T., Okamura, M., Tobita, T. and Torres, A. (2010). Description and analysis of geotechnical aspects associated to the large 2010 Chile earthquake. *Obras y Proyectos* **8**, 25-36

Villavicencio, G., Espinace, R., Palma, J., Fourie, A. and Valenzuela, P. (2014). Failures of sand tailings dams in a highly seismic country. *Canadian Geotechnical Journal* **51**(4), 449–464

Yerro, A., Alonso, E. and Pinyol, N. (2013). The Material Point Method: A promising computational tool in Geotechnics. *18th International Conference on Soil Mechanics and Geotechnical Engineering*, Paris, France, 853–856

Zabala, F. and Alonso, E.E. (2011). Progressive failure of Aznalcóllar dam using the material point method. *Géotechnique* **61**(9), 795–808

Zienkiewicz, O.C. and Shiomi, T. (1984). Dynamic behaviour of saturated porous media: the generalized Biot formulation and its numerical solution. *International Journal for Numerical and Analytical Methods in Geomechancs* **8**(1), 71–96